

# Two kinds of crystalline state of InSb epilayers on GaAs substrates by metalorganic chemical vapor deposition

Shuwei Li <sup>\*</sup>, Yongqiang Ning, Tianming Zhou, Yixin Jin, Yuan Tian

*Changchun Institute of Physics, Academia Sinica, 130021 Changchun, People's Republic of China*

Received 2 May 1996; accepted 22 July 1996

## Abstract

InSb epilayers were grown on GaAs substrates by atmospheric pressure metalorganic chemical vapor deposition (MOCVD). The surface and subsurface morphologies of InSb epilayers were observed by scanning electron microscopy (SEM) and scanning electron acoustic microscopy (SEAM), and the crystalline properties were characterized by the single-crystal X-ray diffraction pattern and double-crystal X-ray rocking curve. Two types of crystalline state after the release of the large compression stress, one was homogeneous dislocation array and the other was heterogeneous plastic flow, were observed and discussed. © 1997 Elsevier Science S.A.

*Keywords:* Semiconductors; Chemical vapour deposition; Surface and interface states; Epitaxy

## 1. Introduction

Recently, growth of InSb epilayers on GaAs substrates (lattice mismatch, 14.5%) has attracted much attention [1,2]. The interest is generated by their potential uses as infrared detectors, high-speed circuit elements and magnetic Hall devices because of narrow bandgap, low electron effective mass and large mobilities. The use of GaAs substrate is interesting because a wide bandgap and semi-insulating substrate facilitates electrical isolation, decreases parasitic capacitances, and allows for the integration of infrared detection and signal processing circuits on the same substrate. In the other hand, the material information of high lattice-mismatched InSb/GaAs heterojunction provides a further contribution to rapidly growing data base relating to strained-layer systems [3]. The performance of the devices is often limited by the mechanical properties of both the films and the structures to which they are attached. Stresses which arise during the epitaxial growth can lead to deformation and failure. Scanning electron acoustic microscopy (SEAM) was developed in 1980 [4,5] and has been mainly used in the last few years in the characterization of many materials. It is a new method to study crystalline quality, defect and plastic flow of the semiconductor epilayers for novel optoelectronic devices and monolithic integration of optoelectronic devices [6]. In our paper, InSb epilayers on the GaAs substrates were

characterized by single-crystal X-ray diffraction pattern and double-crystal X-ray rocking curve, and the subsurface information of crystalline quality and plastic flow were observed and studied by SEAM. Two kinds of the crystalline state, the homogeneous and the heterogeneous, were discussed.

## 2. Epitaxial growth

The InSb epilayers were grown on the GaAs substrates by metalorganic chemical vapour deposition (MOCVD) using a conventional atmospheric pressure horizontal reactor. The sources of In and Sb were trimethylindium (TMIn) and trimethylantimony (TMSb), respectively. TMIn and TMSb were respectively held at 17 °C and –10 °C by using temperature baths and carried by Pd-diffused hydrogen into reactor. The substrates were semi-insulating GaAs which were oriented 2–3° off (100) towards <110>. GaAs substrates were cleaned by degreasing in solvents and deionized water. They were then chemically polished by solution of H<sub>2</sub>O<sub>2</sub>:H<sub>2</sub>O:H<sub>2</sub>SO<sub>4</sub> = 1:1:3 for 3 min, rinsed with deionized water and blown dry with nitrogen to put into the reactor. III/V ratio ( $P = P_{\text{TMIn}}/P_{\text{TMSb}}$ ) were varied from 0.3 to 1.5. The total gas flow into the reactor was 41 min<sup>-1</sup>. The growth temperature of InSb buffers was in 420 °C and the growth time was 10 min. The growth temperatures were varied from 500 to 520 °C and the growth times were varied from 60 to 180 min. Because the melting point of InSb alloy is at 525

<sup>\*</sup> Corresponding author.

°C, the epilayer growth temperature should be below this temperature. But, TmIn and TMSb pyrolysis will decrease with decreasing growth temperature. The buffer growth mode was used to achieve good surface morphology and increased crystalline quality of the InSb epilayer [7].

### 3. Characterization of the films

Fig. 1(a) shows a scanning electron microscopy (SEM) image of No. 1 InSb epilayer. On the surface, a misfit dislocation network of orthogonal array can be observed. The dislocation was Lomer–Cottrell sessile  $90^\circ$  and Burgers vectors of dislocations were  $a/2\langle 110 \rangle$  and  $a/2\langle \bar{1}10 \rangle$ . At same time, a 3D island nucleus with bright spots can be also observed. Fig. 1(b) presented the single-crystal X-ray diffraction patterns, and the full width of half-maximum (FWHM) is 24 arcmin of the Cu  $K\alpha_1$  diffraction peak. The X-ray diffractometer was a D/max-rA, the radiation emitted by Cu  $K\alpha$  was in 40 kV and from 10 to 50 mA, and the slit was DS/SS =  $0.5^\circ$  and RS = 0.15 mm. The epilayer with high crystalline quality had been obtained because the Cu  $K\alpha_1$  diffraction peak separated from Cu  $K\alpha_2$  diffraction peak. Fig. 1(c) the double-crystal X-ray rocking curve was measured by a scanning-type double-crystal topographic goniometer which worked in the radiation emitted by Cu  $K\alpha$  was in 40 kV and 100 mA. In Fig. 1(c) the double-crystal X-ray rocking curve, the FWHM of the curve was 28 arcmin, which

illustrates a good crystalline quality of epilayer since the double-crystal X-ray rocking curve of the InSb/GaAs heterojunction is very difficult to obtain. The double-crystal X-ray rocking curve especially fit small lattice-mismatch epilayers. Because the lattice-mismatch between the InSb epilayer and GaAs substrate is very large, an epilayer of high crystalline quality is difficult to grow.

Fig. 2(a)–2(c) were No. 2 InSb epilayer images of scanning electron acoustic microscopy (SEAM). SEAM has been successively reported as a new experimental tool for the study of polarization distribution, phase transition, subgrain boundary and domain structure in polar materials and non-destructive observation of internal phenomena in many other materials and devices. We reported that SEAM may observe and study non-destructively the crystalline quality, defect and plastic flow of the epilayers of semiconductors. The set-up of the electron acoustic experiment is constructed using conventional scanning electron microscopy to which several newly designed parts, a flexible plug-in beam blanking system, an opto-electronic coupler and a spring-loaded and metal-shielded PZT (piezoelectric ceramic transducer) electron acoustic signal detector, are attached. A chopping system consisting of a pair of condenser plates and a flexible plug-in beam blanking electronics to create a periodically modulated beam is used. The chopping electron beams generate both acoustic and thermal waves in samples clamped on a PZT, which is often explained by the conversion of an electron-beam-induced heat distribution by means of the ther-

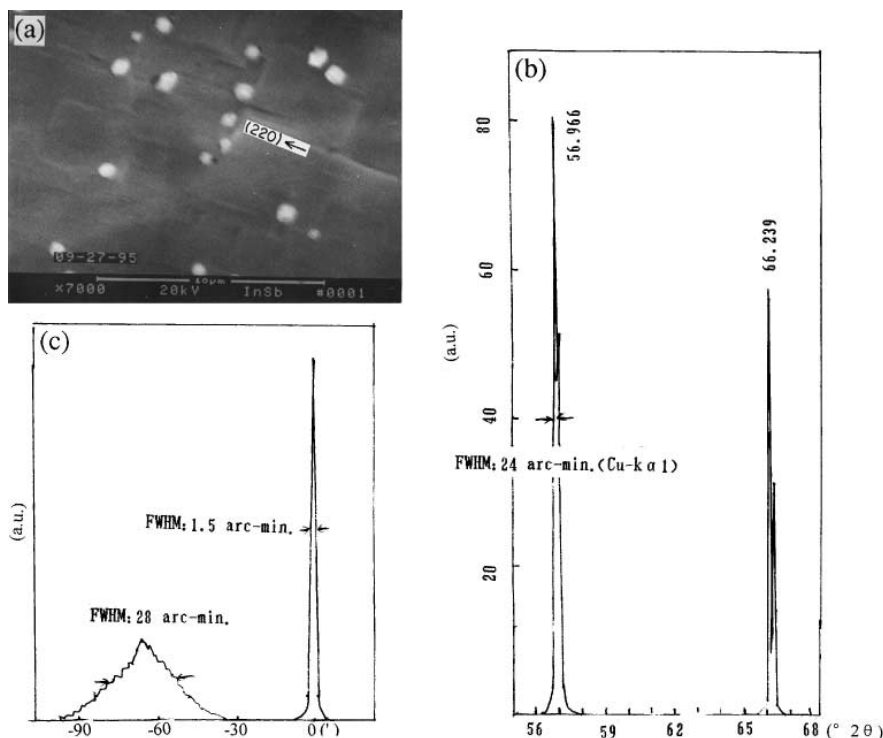


Fig. 1. No. 1 InSb/GaAs heterojunction: growth time, 90 min; growth temperature, 500 °C; III/V ratio, 0.5. (a) SEM image of InSb/GaAs. The Lomer–Cottrell sessile  $90^\circ$  dislocations formed well-distributed dislocation network and were incorporated into the edge of 3D islands. The crystalline state is in homogeneous way. (b) Single-crystal X-ray diffraction patterns and shows a high quality epilayer. (c) Double-crystal X-ray rocking curve (400) and shows a good crystalline state.

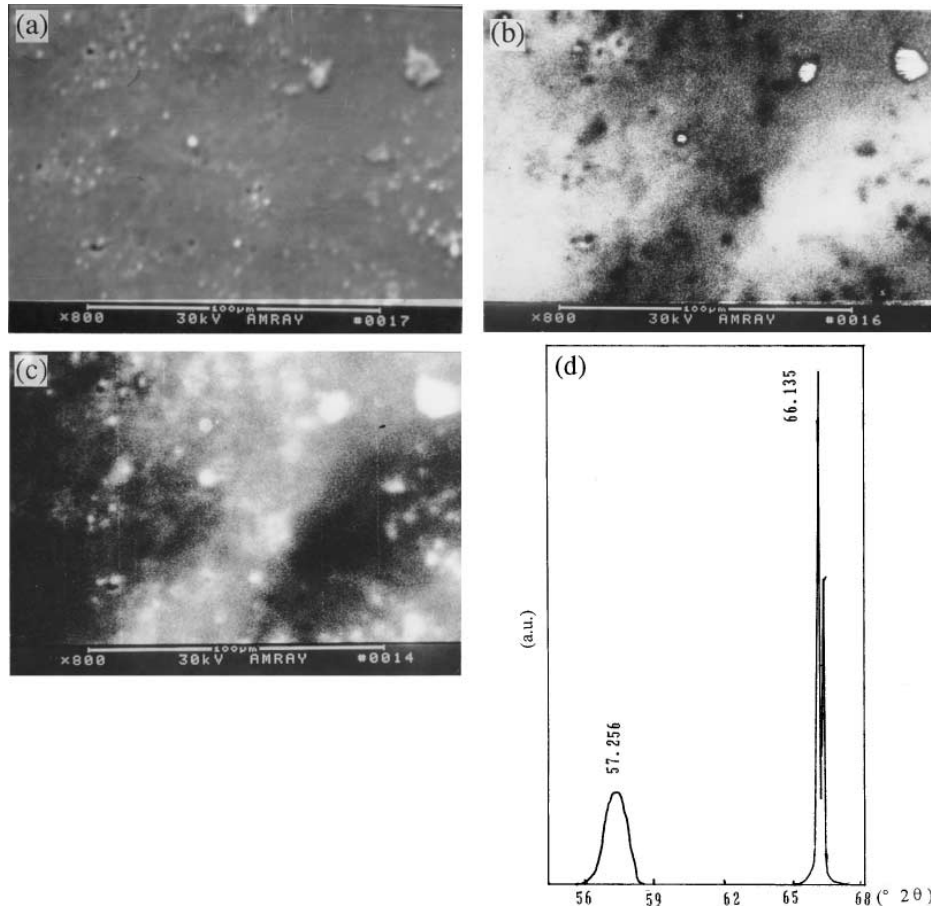


Fig. 2. No. 2 InSb/GaAs heterojunction: growth time, 180 min; growth temperature, 520 °C; III/V ratio, 1.2. (a) SEM image, and (b) and (c) two SEAM images in situ. The plastic flow was changed from (c) to (b) and disappeared in the surface, and the twins or defects were changed from (c) to (a), which showed two techniques provided different information. The single-crystal X-ray diffraction patterns shows a poor quality. The crystalline state was heterogeneous. (a) Scanning electron microscopy (SEM); (b) scanning electron acoustic microscopy (SEAM)  $f=180.7$  kHz; (c) scanning electron acoustic microscopy (SEAM)  $f=109$  kHz; (d) single-crystal X-ray diffraction patterns.

mal expansion coefficient. The thermal wave component generated in the material is highly attenuated, in practice, and the information recorded from the transducer attached to a thermally thick sample depends on the received acoustic wave component. The electron beam characteristics were chopping frequency from 30 to 500 kHz, duty ratio of 50%, acceleration voltage of 20–30 kV, and maximum beam current of  $4 \times 10 \mu\text{A}$ . In Fig. 2, the growth time of the heterojunction was 180 min, III/V ratio was 1.2, and the thicknesses of the film was  $7 \mu\text{m}$ . Fig. 2(a) presented a SEM image and Fig. 2(b) and 2(c) were two SEAM images in situ. The crystal slab thicknesses of the subsurface (Fig. 2(b) and 2(c)) were 3.8 and  $5.6 \mu\text{m}$ . Plastic flows (the boundary between the bright and the dark) and many twins or defects which relieved the huge lattice-mismatch stretched right to the epilayer surface (Fig. 2(a)) SEM image. The size of the twins or defects were changed from Fig. 2(c) to Fig. 2(a), and the plastic flow was changed and disappeared in the Fig. 2(a) surface, which showed two techniques provided different information. Fig. 2(d) was the single-crystal X-ray diffraction pattern of No. 2 sample to show the crystalline quality. The radiation emitted by  $\text{Cu K}\alpha_1$  of the single-crystal

X-ray diffraction pattern did not separate from the  $\text{Cu K}\alpha_2$  radiation, and the FWHM of the diffraction pattern was very wide due to mixing of  $\text{Cu K}\alpha_1$  and  $\text{Cu K}\alpha_2$ . The very wide double-crystal X-ray rocking curve illustrated a poor crystalline quality.

#### 4. Experimental discussion

Two kinds of the crystalline state due to two different stress-driven mass transport processes to release the huge compression stress were involved. The samples in Figs. 1 and 2 presented two different distributions of the crystalline state. In Fig. 1(a) the Lomer–Cottrell sessile  $90^\circ$  dislocation (dislocation Burgers vectors are  $a/2\langle 110 \rangle$  and  $a/2\langle \bar{1}\bar{1}0 \rangle$ ) formed orthogonal array on the surface of the SEM image [8,9]. The many white spots were InSb 3D island nuclei. The release of huge compression stresses was considered as homogeneous because of the well-distributed dislocation networks observed by SEAM and the high crystalline quality obtained by the very narrow single-crystal X-ray diffraction pattern and double-crystal X-ray rocking curve. During ther-

modynamic growth, at the beginning of the deposition in the two-dimensional growth mode (2D way), the strain energy increased with epilayer thickness until the generation of the misfit-relieving dislocation at very thin critical thickness  $h_c$  in this high misfit system [10]. Then, the epitaxial growth was in the Stranski–Krastanov mode (2D–3D way), 3D islands were formed to develop, and the plastic relaxation begun through the nucleation of misfit dislocations [11]. The strain-relaxed islands grew, and the sessile  $90^\circ$  dislocations were incorporated into the edge of the growing island shown in Fig. 1(a) [9]. Direct formation of  $90^\circ$  dislocations had been previously suggested only in systems with large mismatch [12]. Fig. 1 showed that the well-distributed dislocation network formed a orthogonal array to release mainly huge compression stress in a homogeneous way.

In Fig. 2 it was shown that the other stress-driven mass transport processes lead to the macroscopic heterogeneous plastic deformation. Because the acoustic wave of SEAM is a Rayleigh wave which is especially sensitive to variations in elastic properties, the boundary between the bright and the dark regions were regarded as the plastic flows in Fig. 2(c) and 2(b) SEAM images. They were changed from the deep crystal slab of the buried subsurface (Fig. 2(c)), an image of electron acoustic waves  $f=109$  kHz and  $d=5.6$   $\mu\text{m}$ , and the other deep crystal slab (Fig. 2(b)),  $f=180.7$  kHz and  $d=3.8$   $\mu\text{m}$ , to the surface (Fig. 2(a)) SEM image where the plastic flows cannot be observed, which showed the different imaging mechanisms of SEM and SEAM. From Fig. 2(c), 2(b) and 2(a), the three-dimensional change of the plastic flow was observed; at same time, the change of twins or defects was also observed. The heterogeneous multiplication of misfit dislocation formed plastic flows to release stress as the other way due to the change of thermodynamics such as the temperature and III/V ratio. The plastic flows influenced seriously the crystalline quality, and in Fig. 2(d), the X-ray diffraction pattern with the very wide FWHM diffraction peak. The Fig. 2(d) X-ray diffraction showed internal crystalline information; as other experiment methods, the Fig. 2(c) and 2(b) SEAM images and Fig. 2(a) SEM image showed vividly that the crystalline state after the release of large compression was the heterogeneous due to the change of the plastic flows from the very deep buried subsurface to

the surface. It is clear that the former growth way, the homogeneous, is expected during the epitaxial growth.

## 5. Conclusion

In this paper two kinds of crystalline state of InSb epilayers on GaAs substrates were grown by MOCVD, and studied by SEM, X-ray diffraction patterns and SEAM. The crystalline state of the homogeneous and the heterogeneous to release huge compression stress were discussed. The 3D islands, twins and elastic flows in the so-high misfit system were the first observed by SEAM.

## Acknowledgements

The authors wish to thank Fuming Jing, Qingrui Yin and Bingyang Zhang of Shanghai Institute of Ceramics, Academia Sinica for the SEAM experiment.

## References

- [1] M. Bchet, B. Stoll and K. Heime, *J. Crystal Growth*, **135** (1994) 434–440.
- [2] K.C. Baucom and R.M. Biefeld, *Appl. Phys. Lett.*, **64** (22) (1994) 3021–3023.
- [3] G.M. Williams, C.R. Whitehouse, C.F. McConville, A.G. Cullis and T. Ashley, *Appl. Phys. Lett.*, **53** (13) (1988) 1189.
- [4] G.S. Cargill III, *Nature*, **286** (1980) 691–693.
- [5] M. Urchulutegui and J. Piqueras, *J. Appl. Phys.*, **67** (1) (1990) 1–4.
- [6] Shuwei Li, Yixin Jin, Tianming Zhou, Baolin Zhang, Yongqiang Ning, Hong Jiang, Guang Yuan, Xinyi Zhang and Jinshan Yuan, *J. Cryst. Growth*, **156** (1995) 39–44.
- [7] R.M. Biefeld and G.A. Hebner, *J. Crystal Growth*, **109** (1991) 272–278.
- [8] D. Hull and D.J. Bacon, *Introduction to Dislocations*, Pergamon Press, Oxford, p. 106.
- [9] F.K. LeGoues, J. Tersoff, M.C. Reuter, M. Hammer and R. Tromp, *Appl. Phys. Lett.*, **67** (16) (1995) 2317.
- [10] M. Lentzen, D. Gerthsen, A. Forster and K. Urban, *Appl. Phys. Lett.*, **60** (1) (1992) 74–77.
- [11] Y. Androussi and Lefebure, *Appl. Phys. Lett.*, **65** (9) (1994) 1162–1164.
- [12] A. Sakai and T. Tatsumi, *Phys. Rev. Lett.*, **71** (1993) 4007.